Inorg. Chem. **2008**, *47*, 8487−8497

Forum

Status of Trivalent Copper and Charge-Transfer Excitons in High-T_C Cuprates

Michel Pouchard,* Jean-Pierre Doumerc, and Antoine Villesuzanne

ICMCB, CNRS, Bordeaux I University, 87 Av. Dr. A. Schweitzer, 33608 Pessac Cedex, France

Received June 5, 2008

A chemical bonding approach based on tight-binding cluster and band calculations, taking into account on-site Coulomb repulsion (Hubbard *U* parameter) to differentiate doubly and singly occupied states, was applied to high-T_C superconducting cuprates and related compounds. This work provides rational insight and explanations for issues such as (i) the actual oxidation number Cu^{I+} for formally trivalent copper in oxides such as $La_2Li_{1/2}Cu_{1/2}O_4$, (ii) the dominant oxygen character of the doping holes in $(CuO_2)^{n-}$ planes, (iii) the Mott−Hubbard character of the insulator-to-metal transition triggered by hole doping, leading to an oxygen-to-copper charge transfer of avalanche type, (iv) the occurrence of an excitonic phase with anisotropic Frenkel-type excitons, (v) the role of Coulomb interactions between excitons and between doping holes and their exciton surroundings, and (vi) the on-time pairing of doping holes by means of an "excitonic glue".

1. Introduction

More than 20 years ago, Bednorz and Müller were at the origin of one of the most exciting adventures of 20th century scientific research, with the discovery of high-T_C superconductivity (HT_C) in the family of double oxides of cuprate type.[1] One of the major consequences of what was termed by Müller himself as the "golden rush" was a closer collaboration of the physicist and chemist communities, already initiated 20 years earlier around the remarkable properties of vanadium oxides, which could exhibit insulator-to-metal transitions characterized by resistivity drops of more than 10 orders of magnitude.[2]

The origin of this high-T_C superconductivity is still debated, but a majority of physicists consider today that it is not of the conventional BCS-type electron−phonon coupling.[3]

Our purpose is not to make an exhaustive review of the many proposed models or to describe all of the new cuprates that have allowed T_C to be increased from about 20 K up to almost 150 K. The aim of this paper is to stress the initial contribution of solid-state chemists and some simple ideas, based on chemical bonding, according to the remarks of physicists like Dagotto or Emery, who pointed out recently that "*such materials display substantial structure in both real space and momentum space. As a consequence the conventional theory must be abandoned.*".[4−6]

Nowadays, the most performing electronic structure calculation methods such as density functional theory, with possible extensions beyond the mean-field approximation, for example, LDA+U (local density approximation with Hubbard-type correction for chosen orbitals) or dynamical mean-field theory,[7] actually describe electrons in both real and momentum spaces (for example, distribution in electron density and Fermi surface).

The simplest approach of solid-state chemists is rather of the tight-binding type and, on the contrary, starts from atomic orbital basis sets, modulated by plane waves leading to Bloch functions, a view closer to real space. However, this approach

* To whom correspondence should be addressed. E-mail: pouchard@icmcb-bordeaux.cnrs.fr. Tel.: +33 540 008 459. Fax: +33 540 008 373.

(1) Bednorz, J. G.; Müller, K. A. *Z. Phys. B: Condens. Matter* **1986**, *64*, 189.
(2) Pouchard, M.; Launay, J.-C. *Mater. Res. Bull.* **1973**, *8*, 95.
(3) Bardeen, J.; Cooper, L. N.; Schrieffer, J. R. *Phys. Rev.* **1957**, *108*, 1175.
(4) Cho, A. *Science* **2006**, *314*, 1072.
(5) Emery, V. J.; Kivelson, S. A.; Tranquada, J. M. *Proc. Natl. Acad. Sci. U.S.A.* **1999**, *96*, 8814.
(6) Buchanan, M. *Nature* **2001**, *409*, 8.
(7) Kotliar, G.; Vollhart, D. *Phys. Today* **2004**, *57*, 53.

10.1021/ic801031y CCC: $40.75
Published on Web 09/29/2008

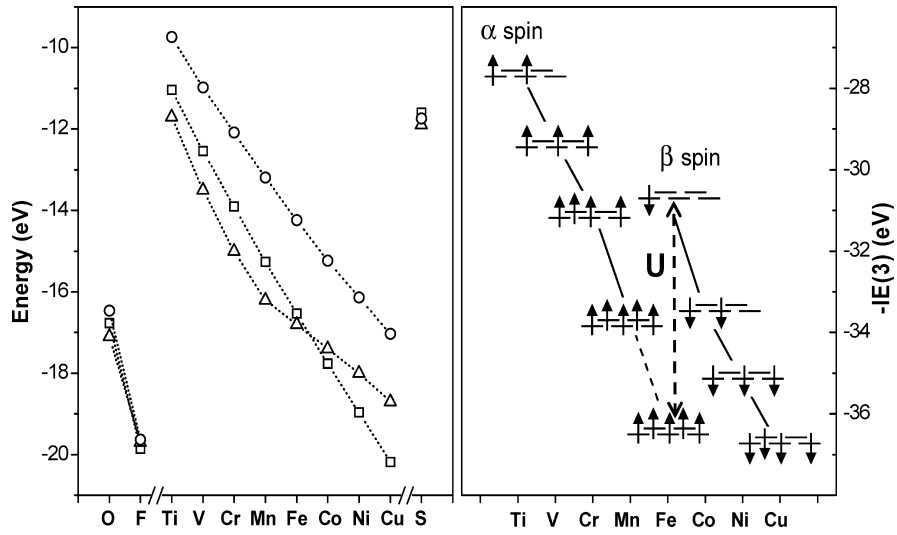

Figure 1. Variation of (left) 3d energy levels, given here by their Coulomb integral H_{dd} according to their tabulations in refs 8 (triangles), 9 (squares), and 10 (circles) and (right) the third ionization energy. The latter shows a sharp discontinuity (U) between $3d^5$ and $3d^6$ configurations of the $M^{2+}(g)$ ion.

must be improved qualitatively by taking into account the exchange-correlation energy (U), in order to differentiate the energy of singly occupied versus doubly occupied states. This is required by the narrow character of the 3d bands in these types of transition-metal oxides (TMOs). The role of U clearly appears in Figure 1, where the smooth variation of the 3d orbital energy (H_{dd})[8−10] with the atomic number Z is compared with that of the third ionization energy IE(3). IE(3) corresponds to the equation

$$M^{2+}(g) \rightarrow M^{3+}(g) + e^-$$

In an ionic model, minus IE(3) gives the 3d orbital energy for the free $M^{2+}(g)$ ion. In the 3d series, the discontinuity observed for IE(3) between Mn^{2+} ($3d^5$) and Fe^{2+} ($3d^6$) illustrates the fact that the sixth electron of Fe, of spin noted β, is less stable by more than 4 eV than the other five electrons of opposite spin (noted α), because of exchange-correlation phenomena (summed up in U).

The main types of equilibria involving electronic transfers, with the exception of intra-atomic spin equilibria, allow differentiation of two types of TMOs in a classification independently proposed by Torrance et al.[11] and by Zaanen et al.:[12]

(i) Mott−Hubbard insulators, where the energy gap U_H between the two Hubbard bands corresponds to the redox equilibrium

$$M^{n+} + M^{n+} \leftrightarrow M^{(n+1)+} + M^{(n-1)+}$$

which is, for chemists, a disproportionation equilibrium.

(ii) Charge-transfer insulators, where the energy gap Δ between oxygen-character valence bands and upper, metal-character Hubbard bands corresponds to the redox equilibrium

$$O^{2-} + M^{n+} \leftrightarrow O^- + M^{(n-1)+}$$

According to a broad consensus, copper oxides belong to the charge-transfer class ($\Delta < U_H$).

In this paper we will try, by means of a chemical approach, to answer questions such as the following:

(1) Does Cu^{III+} really exist?

(2) Why, in the case of p-doped cuprates(II+), are the holes mainly located on O atoms, as demonstrated by X-ray absorption spectroscopy (XANES) at Cu L and O K edges[13−18] or in recent calculations by Lee and Hoffmann?[19] What is then the true oxidation state of copper in these types of phases?

(3) What is the origin of holes pairing in HT_C cuprates and the explanation for the pair weak coherence length (ξ), on the order of the nanometers, compared to its value in conventional BCS-type superconductors?

(4) What is the relation between heterogeneities at the nanometric scale, such as stripes,[5] and the fundamental mechanisms of superconductivity?

The purpose here is not to propose an nth mechanism for HT_C but rather to provide a detailed description of the role of chemical bonding between Cu and O atoms and of the continual, and complementary, back and forth passage between real and momentum spaces (in other words, between chemistry and physics descriptions). We attempt to bring a

(8) Pyykkoe, P.; Lohr, L. L., Jr. *Inorg. Chem.* **1981**, *20*, 1950.
(9) Clementi, E.; Roetti, C. *At. Data Nucl. Data Tables* **1974**, *14*, 177.
(10) Values from the Amsterdam Density Functional program (ADF), as tabulated in the CAESAR package: Dai, D.; Ren, J.; Liang, W.; Whangbo, M.-H. http://www.primec.com.
(11) Torrance, J. B.; Lacorre, P.; Asavaroengchai, C.; Metzger, R. M. *J. Solid State Chem.* **1991**, *90*, 168.
(12) Zaanen, J.; Sawatsky, G. A.; Allen, J. W. *Phys. Rev. Lett.* **1985**, *55*, 418.
(13) Kuiper, P.; van Elp, J.; Sawatsky, G. A.; Fujimori, A.; Hosoya, S.; de Leeuw, D. M. *Phys. Rev. B* **1991**, *44*, 4570.
(14) Bianconi, A.; Budnick, J.; Flank, A. M.; Fontaine, A.; Lagarde, P.; Marcelli, A.; Tolentino, H.; Chamberland, B.; Michel, C.; Raveau, B.; Demazeau, G. *Phys. Lett. A* **1988**, *127*, 285.
(15) Pellegrin, E.; Chen, C. T.; Zaanen, J.; Finck, J. *Physica B* **1995**, *208*, 487.
(16) Hu, Z.; Kaindl, G.; Warda, S. A.; Reinen, D.; de Groot, F. M. F.; Müller, B. G. *Chem. Phys.* **1998**, *232*, 63.
(17) Yarnoff, J. A.; Clarke, D. R.; Drube, W.; Karlsson, U. D.; Taleb-Ibrami, A.; Himpsed, F. J. *Phys. Rev. B* **1987**, *36*, 3967.
(18) Nücker, N.; Finck, J.; Fuggle, J. C.; Durham, P. J.; Timmerman, W. N. *Phys. Rev. B* **1988**, *37*, 5158.
(19) Lee, K. H.; Hoffmann, R. *J. Phys. Chem. A* **2006**, *110*, 609.

new light on the unique features of mixed-valent (II+/III+) cuprate oxides, which were developed notably by Raveau's group in Caen[20] at the beginning of the 1980s.

2. Does Cu^{III+} Really Exist?

For copper, the III+ oxidation state corresponds to a $3d^8$ configuration, analogous to that of Ni^{II+}, which is particularly stable and found in most of its compounds. However, Cu^{III+} has remained unknown for a long time.

The first attempts to stabilize it took place in Germany in Klemm's inorganic chemistry group at Munster and later in Hoppe's group at Giessen.

The first strategy consisted of taking advantage of the very strong oxidizing power of fluorine and led in the 1950s to paramagnetic double fluorides such as K_3CuF_6.[21,22]

The second strategy was to combine a hypothetical binary oxide "Cu_2O_3" of high valency, and hence light acidity, with a strongly basic oxide such as A_2O (A = Na, K, Rb, or Cs), in order to stabilize Cu^{III+} in an oxysalt $ACuO_2$. In these oxides, the Cu atoms occupy square-planar sites, which stabilizes the so-called low-spin (LS) d^8 configuration ($t_{2g}^6 d_{z^2}^2 d_{x^2-y^2}^0$), which is diamagnetic ($S = 0$) and leads to an insulating state.[23]

At the beginning of the 1970s, the inorganic chemistry group in Bordeaux proposed some complementary empirical rules to enhance the stability of Cu^{III+}:

(i) In the case of oxides, adding to Hoppe's strategy, the synthesis under oxygen high pressures generated, for example, in the solid state by the thermal in situ decomposition of $KClO_3$ (Demazeau's thesis[24]).

(ii) Stabilizing ($\sigma^*_{eg}{}^2$) electrons in a half-filled broad band (thanks to an increase of the kinetic energy and to the essentially nonbonding bottom of the band) should lead to a stable metallic state, in a manner similar to the stabilization of W^{V+} in oxide tungsten bronzes Na_xWO_3. In this way, the $LaCuO_3$ perovskite[25] and the first term ($n = 1$) of the Ruddlesden−Popper oxide series $A_{n+1}B_nO_{3n+1}$ such as $LaSrCuO_4$,[26] both metallic conductors and weakly paramagnetic, were predicted and synthesized. The search for isolated clusters of the $(CuO_4)^{5-}$ type presented a fundamental interest for the characterization of LS Cu^{III+}. Substituting Li^+ ions in place of Cu^{III+} in $LaSrCuO_4$, in a 1:1 ordered structure, was expected to lead to an equatorial compression and hence to a strong elongation of the CuO_6 octahedron, resulting in a nearly square-planar environment, hence stabilizing the diamagnetic LS d^8 configuration. $La_2Li_{0.5}Cu_{0.5}O_4$ was actually synthesized and characterized[27] (Figure 2), and the Li/Cu ordering was confirmed later on.

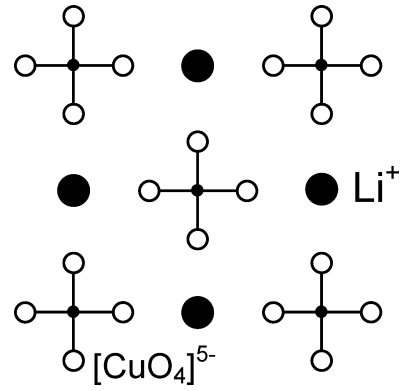

Figure 2. Representation of the (001) perovskite-type layer of La_4LiCuO_8, showing the 1:1 ordering of $(CuO_4)^{5-}$ entities and Li ions.

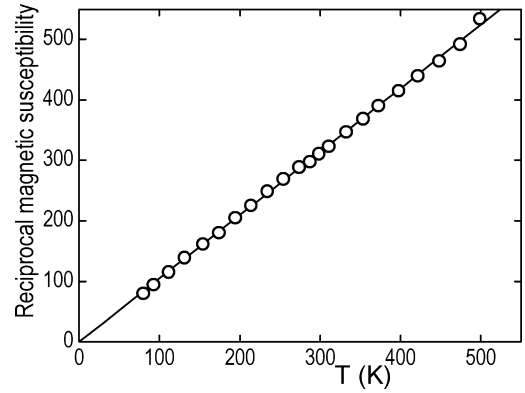

Figure 3. Thermal variation of the reciprocal magnetic susceptibility for the fluoride Na_3CuF_6 (from ref [28]), with an effective moment of 2.77 μ_B in good agreement with the theoretical value of 2.83 μ_B for $S = 1$ Cu^{III+}.

(iii) In the case of fluorides, very pure phases free of Cu^{2+}, such as Na_3CuF_6, were prepared;[28] their magnetic characterization revealed a Curie constant very close to 1 ($\mu_{eff} = 2.77\ \mu_B$, in good agreement with the theoretical value $\mu_{th} = 2.83\ \mu_B$ for spin $S = 1$; Figure 3). In these fluorides, Cu^{III+} possesses then the high-spin (HS) configuration $t_{2g}^6 d_{z^2}^1 d_{x^2-y^2}^1$, that is, the most common configuration for a d^8 ion. Two reasons can explain this result:

(1) F 2p orbitals are particularly stable, more than Cu 3d orbitals [$H_{dd}(Cu) = -18.7$ eV; $H_{pp}(F) = -19.7$ eV[9]]. F 2p orbitals constitute then the basis for the bonding molecular orbitals (MOs) of the $(CuF_6)^{3-}$ cluster, an usual situation for a transition-metal complex.

(2) F^- ions create a weaker crystal field than O^{2-} ions, and thus the elongation of the $(CuF_6)^{3-}$ octahedron does not provide a large enough stabilization of the d_{z^2} orbital to compensate for the loss of exchange-correlation energy that would induce a $d_{z^2}^2 d_{x^2-y^2}^0$ ($S = 0$) configuration.

Even if recent XANES studies have demonstrated that the Cu−F bonding presented a significant covalent character, we can keep the notion of the III+ oxidation state for copper, and in particular the ionic notation $(CuF_6)^{3-}$ for the fluorides A_3CuF_6.

(20) Nguyen, N.; Studer, F.; Raveau, B. *J. Phys. Chem. Solids* **1983**, *44*, 389.
(21) Hoppe, R. *Angew. Chem.* **1961**, *73*, 30.
(22) Hoppe, R.; Homann, R. *Naturwissenschaft* **1966**, *53*, 501.
(23) Hestermann, K.; Hoppe, R. *Z. Anorg. Allg. Chem.* **1969**, *367*, 249.
(24) Demazeau, G. Ph.D. Thesis, University of Bordeaux, Bordeaux, France, 1973.
(25) Demazeau, G.; Parent, C.; Pouchard, M.; Hagenmuller, P. *Mater. Res. Bull.* **1972**, *7*, 913.
(26) Goodenough, J. B.; Mott, N. F.; Pouchard, M.; Demazeau, G.; Hagenmuller, P. *Mater. Res. Bull.* **1973**, *8*, 647.
(27) Goodenough, J. B.; Demazeau, G.; Pouchard, M.; Hagenmuller, P. *J. Solid. State Chem.* **1973**, *8*, 325.
(28) Grannec, J.; Portier, J.; Pouchard, M.; Hagenmuller, P. *J. Inorg. Nucl. Chem. Suppl.* **1976**, *119*.

Table 1. Orbital Energy Parameters (from Ref 9) Used in EHTB Calculations for the $(CuO_4)^{5-}$ Cluster

	Cu 4s	Cu 4p	Cu 3d
H_{ii}(eV)	−7.44	−4.26	−18.70
	O 2s	O 2p	
H_{ii}(eV)	−33.70	−17.10	

What about the case of oxides formally Cu^{III+}? Since our early works in the 1970s, these compounds have been widely studied to serve as reference compounds with respect to HT_C cuprates.

All X-ray photoelectron spectroscopy or XANES studies at Cu K and L edges and at the O K edge have shown that the holes were mainly located on the O atoms. The Cu^{III+} state is then described as a mixture of configurations written as

$$a|3d^8\rangle + b|3d^9\underline{L}\rangle$$

where $b \gg a$ and $\underline{L}$ stands for a hole on the oxygen ligand, i.e., O^-.

According to this picture, the diamagnetism of $La_2Li_{0.5}Cu_{0.5}O_4$ could be explained by a strong local antiferromagnetic coupling between the $S = {}^1/_2$ unpaired electrons of Cu^{2+} and O^- ($2p^5$) or in a way similar to the Zhang and Rice singlet resulting from bonding hybridization.[29] Because such an explanation does not seem very convincing to us, we carried out a MO calculation by the extended Hückel tight-binding method (EHTB)[30] for a $(CuO_4)^{5-}$ square-planar cluster using the atomic orbital energies given in Table 1. Note that H_{dd}(Cu) is lower than H_{pp}(O) in other parameter sets also (Figure 1).

Figure 4 displays the results of these calculations and suggests the following comments:

(i) Five Cu 3d orbitals, more stable than the 12 O 2p orbitals, constitute the basis for bonding MOs at about −19 eV. The maximum splitting between them [$\sigma^L_{x^2-y^2}$(Cu−O) and $\pi^L_{xz,yz}$ (Cu−O)] does not exceed 0.5 eV; we shall later on label them b_{1g}(Cu−O) and e_g(Cu−O) according to D_{4h} group notation. The weak splitting results from a crystal-field attenuation by covalency.

(ii) The 12 O 2p orbitals are divided into two sets: (1) the antibonding ones, denoted (O−Cu)*, with a dominant oxygen character and with a symmetry adapted to that of Cu d orbitals and (2) the other seven (orthogonal to the previous ones) with a purely oxygen character and denoted (O−O) or (O−O)*, according to their bonding or antibonding character, respectively.

(iii) The antibonding MO (O−Cu)* are sorted by increasing energy according to π^*_{xy}, denoted b_{2g}(O−Cu)*, $\sigma^*_{z^2}$, denoted a_{1g}(O−Cu)*, $\pi^*_{xz,yz}$, denoted e_g(O−Cu)*, and $\sigma^*_{x^2-y^2}$, denoted b_{1g}(O−Cu)*. Due to the symmetry, a_{1g}(O−Cu)* contains a weak contribution of Cu 4s besides $3d_{z^2}$. The strongly antibonding b_{1g}(O−Cu)* MO is the most destabilized, toward −15 eV.

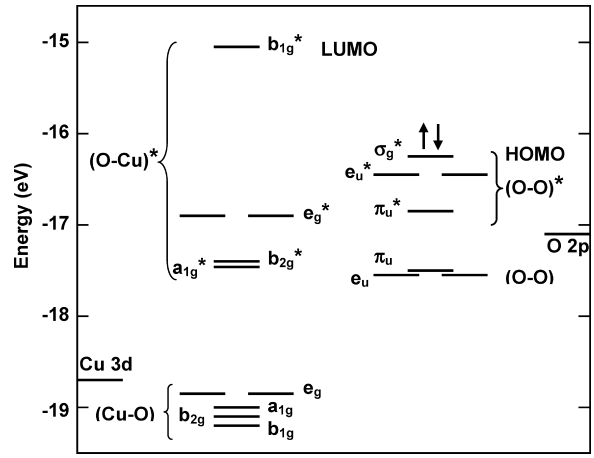

Figure 4. Molecular energy levels for a $(CuO_4)^{5-}$ square-planar cluster (d_{Cu-O} = 1.90 Å), calculated by the extended Hückel method with parameters from Table 1, in D_{4h} group notation. Left: bonding (Cu−O) and antibonding (O−Cu)* levels. Right: the various (O−O) levels with bonding and antibonding characters. For this calculation, singly and doubly occupied states were not differentiated (i.e., $U_H = 0$).

For these (O−Cu)* MOs, the dispersion is much more important (∼2.5 eV) than for that the (Cu−O) MOs with dominant copper character.

(iv) The interactions O 2p−O 2p are strong and, depending on symmetry, can be either bonding (O−O) or antibonding (O−O)*, of the σ or π type. A difference of 1.2 eV is noticed between $2p_\sigma$ and $2p_{\sigma^*}$. The most antibonding MO among them, denoted σ^*_g (at approximately −16.2 eV), corresponds to the highest electronic occupied MO (HOMO). It is doubly occupied and separated by a ∼1 eV gap from the lowest unoccupied MO (LUMO) that corresponds to $b_{1\,g}$(O−Cu)*. The 32 electrons of the $(CuO_4)^{5-}$ cluster, without counting 2s electrons, are distributed in the 16 MOs of lowest energy and thus locate E_F between the σ^*_g and $b_{1\,g}$(O−Cu)* levels. Indeed, this diagram explains the diamagnetic and insulating character of $La_2Li_{0.5}Cu_{0.5}O_4$.

(v) Then, what is the copper oxidation number? With five Cu-based bonding MOs, each doubly occupied, the $3d^{10}$ configuration must be attributed to copper, i.e., Cu^{I+}. However, the strong Cu−O covalency excludes a description in terms of the Cu^+ ion. The two holes (LUMO) correspond to the $b_{1\,g}$(O−Cu)* MO with dominant oxygen character. Despite the strong Cu−O covalency, the polyoxide ion terminology $(O_4)^{6-}$ can be used with, for oxygen, a noninteger oxidation number (−1.50) because the two holes are mainly shared by the four O atoms. This is analogous in principle to the peroxide $(O_2)^{2-}$ ion, where two holes are shared by two O atoms, or as their chalcogenide homologues such as $(S_2)^{2-}$, very stable in pyrites.

In conclusion, Cu^{III+} does really exist in the case of the double fluorides, such as Na_3CuF_6. In oxides, it is more appropriate to evoke Cu^{I+} associated with polyoxide ions.

3. Nature of Doping Holes in the 2D Mixed-Valency (II+/III+) Cuprates

The crystal chemistry of HT_C cuprates corresponds to 2D networks of corner-sharing elongated octahedra, in some cases, square pyramids or planar entities. Here we use a

(29) Zhang, F. C.; Rice, T. M. *Phys. Rev. B* **1988**, *37*, 3759.
(30) (a) Hoffmann, R. *J. Chem. Phys.* **1963**, *39*, 1397. (b) Calculations were done using the CAESAR package: Dai, D.; Ren, J.; Liang, W.; Whangbo, M.-H.; Whangbo, M. H.; Hoffmann, R. *J. Am. Chem. Soc.* **1978**, *100*, 6093, http://www.primec.com.

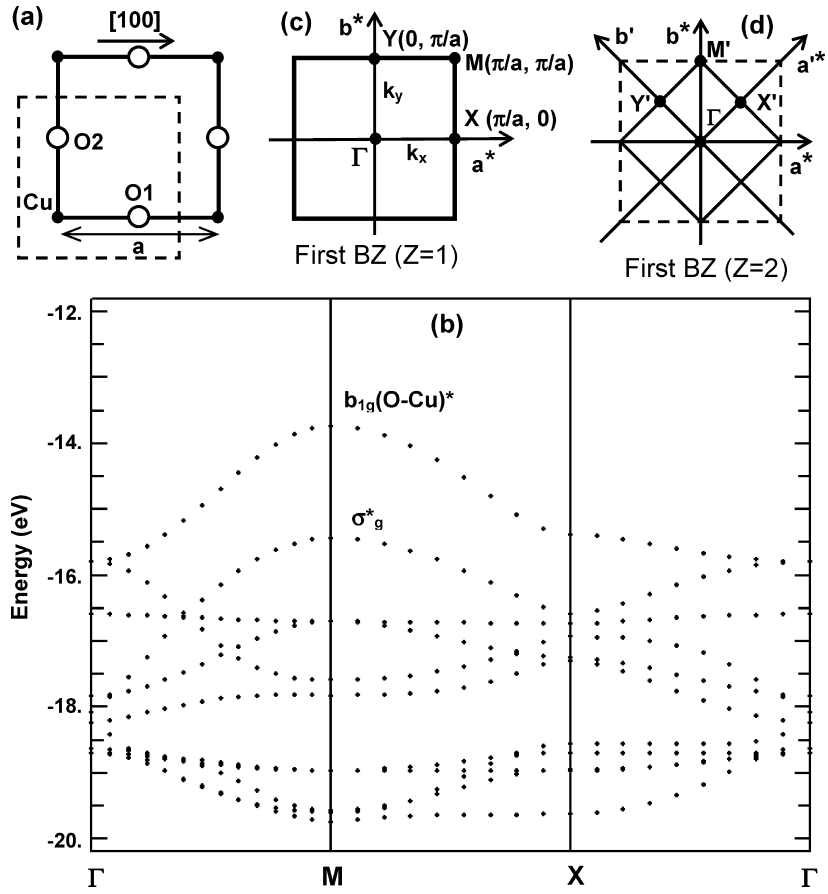

Figure 5. (a) Unit cell for the 2D network of $(CuO_2)^{2-}$ layers. (b) Dispersion curves $E(k)$ obtained by the EHTB method (in the approximation $U_H = 0$) with parameters from Table 1. (c) First BZ for the $a \times a$ unit cell. (d) First BZ for the double cell $a\sqrt{2} \times a\sqrt{2}$ such as, for example, for the antiferromagnetic low-temperature form of La_2CuO_4 (tetragonal approximation).

simplified description of these layers, based on a square unit cell of parameter a ($a = 3.8-3.9$ Å approximately, depending on the composition).

By the way, Hiroi et al.[31] have evidenced the superconducting properties ($T_C = 28$ K) of $Ca_{2-x}Na_xCuO_2Cl_2$ in which CuO_2 layers are capped by Cl atoms. Superconductivity was also found by Zhu et al.[32] in $Tm_{1.83}Ca_{0.17}CuO_4$ ($T_C = 30$ K), of Nd_2CuO_4 structural type in which there is no O atom in the apical position. Finally, $(Ca, Sr)_{1-x}CuO_2$ cuprates, with simple CuO_2 sheets, exhibit superconducting transition temperatures above 100 K.[33]

Superconducting CuO_2 sheets are generally separated along the crystal c direction by electron or hole "reservoir" layers. For oxides derived from La_2CuO_4, these reservoir layers are of three types: $[La_{2-x}A_xO_2]^{(2-x)+}$ (A = Ba, Sr, Ca), $[Ca_{2-x}Na_xCl_2]^{(2-x)+}$ and $[La_2O_{2+\delta}]^{p+}$ with $2(1-\delta) < p < 2-\delta$.

Let us recall that the parent oxide $La_2CuO_{4.0}$ crystallizes at high temperature in the centered space group *I*4/*mmm* but undergoes at low temperature an orthorhombic distortion (space group *Bmab*) with a unit cell doubling. In this distortion, the strongly elongated CuO_6 octahedra undergo an alternate tilting, which allows the elastic strain to relax between the two layer types.[34]

3.1. Band Structure of a $[CuO_2]^{n-}$ Square-Planar Network, Calculated by the EHTB Method. As opposed to the previous case of an isolated cluster, we now have a 2D infinite network, in which two Cu atoms each share O atom. The 17 MO in Figure 4 are then broadened into 11 energy bands per cell, in the considered energy range.

For the simplest unit cell ($Z = 1$) of parameter a (Figure 5a), the dispersion curves $E(k)$ are shown in Figure 5b. The first Brillouin zone (BZ) is shown in Figure 5c, together with some high symmetry points: Γ(0,0), M(π/a,π/a), X(π/a,0), and Y(0,π/a). For Γ and M, the local symmetry is respectively antisymmetric [ungerade (u), as O 2p] and symmetric [gerade (g)].

The analysis of $E(k)$ curves suggests the following comments:

(i) As in the cluster case, the bonding bands, around −19 eV, are of dominant copper character and are weakly dispersed (<1 eV).

(ii) At Γ point, of u symmetry, Cu 3d (g) and O 2p (u) orbitals form nonbonding states. Only the O 2s orbitals are weakly mixed with Cu 3d orbitals.[35]

(iii) As in the cluster case, the five antibonding bands are

(31) Hiroi, Z.; Kobayashi, N.; Takano, M. *Nature* **1994**, *371*, 139.
(32) Zhu, W. J.; Zao, Y. S.; Zhou, X. J.; Yin, B.; Dong, C.; Huang, Y. Z.; Zhao, Z. X. *Physica C* **1994**, *230*, 385.
(33) Hiroi, Z.; Kobayashi, N.; Takano, M. *Physica C* **1996**, *266*, 191.
(34) Goodenough, J. B.; Manthiran, A.; Zhou, X. J. *Mater. Res. Soc. Symp. Proc.* **1989**, *156*, 339.

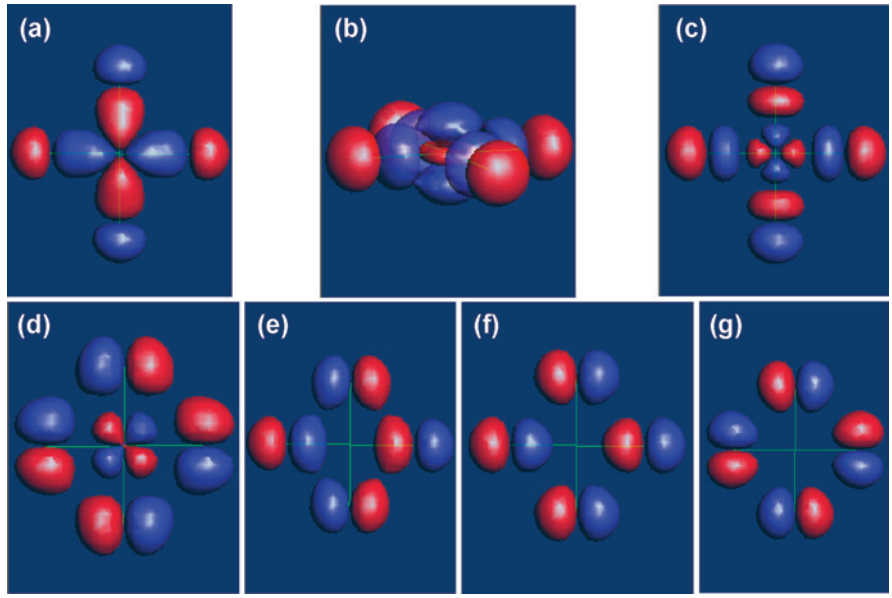

Figure 6. Eight possible combinations of O $2p_{x,y}$ atomic orbitals, with g or u symmetries (corresponding to crystal orbitals at respectively M and Γ points in the BZ). Note the bonding versus antibonding O−O interactions in the orbitals: (a) b_{1g}(Cu−O) with Cu−O bonding character, (b−d) a_{1g}(O−Cu)*, b_{1g}(O−Cu)*, and b_{2g}(O−Cu)* with O−Cu antibonding character, (e) e_u with O−Cu nonbonding character but O−O bonding character, (f) e_u with O−Cu nonbonding but O−O antibonding characters (two degenerate orbitals; only one is shown), and (g) σ^*_g with strong O−O antibonding character.

of dominant oxygen character. A sixth band, of pure oxygen character at the M point, is denoted σ^*_g in relation to its (O−O)* antibonding nature (see Figure 6g). The five (O−Cu)* bands are of pure oxygen character at the Γ point.

(iv) On the basis of the $2p_x$ and $2p_y$ orbitals of the two O atoms in the unit cell, two sets of hybrid orbitals can be constructed: the first one is orthogonal to Cu 3d orbitals at the Γ point, thus of pure oxygen character, and the second one is symmetry-adapted to Cu 3d orbitals (Figure 6). At the Γ point, the energy gap (2.5 eV wide) between (O−O) and (O−O)* σ-type bands is twice the value for the equivalent gap obtained in the cluster case. Indeed, such a gap from bonding to antibonding states is given by $\Delta E = 2z\beta$, where z is the number of first neighbors and β is the resonance integral, denoted t by physicists, for transfer integral; z equals 2 and 4 for the cluster and infinite layer, respectively.

(v) The oxygen character bands have a significant dispersion, of approximately 4.5 eV between −18 and −13.5 eV. In particular, the b_{1g}(O−Cu)* band (∼ 2 eV wide) is characterized by both (O−Cu)* and (O−O)* strong antibonding interactions, as $\beta_{O-O} \sim -0.3$ eV. The oxygen character at the M point can be roughly estimated by summing, after normalization (neglecting overlaps), the square of oxygen coefficients in the expression of the wave function $\Psi_M = -0.547b_{1g} - 0.701p_x(1) + 0.701p_y(2)$, i.e., about 77% in oxygen.

3.2. La_2CuO_4 (*I4/mmm*). At low temperature, the description of the orthorhombic distortion (*Bmab*) and of the antiferromagnetic order of copper spins, coupled with a strong Cu−O−Cu superexchange ($J_{ex} \sim 0.1$ eV), requires a double unit cell ($a\sqrt{2} \times a\sqrt{2}$) and thus a BZ divided by 2 (Figure 5d). For sake of clarity in the diagrams to come, the single unit cell ($a \times a$) will be used. With 21 electrons per cell, without counting O 2s electrons, the Fermi level (E_F) should lie in the middle of the b_{1g}(O−Cu)* band and give a Fermi surface joining X and Y points in the BZ (Figure 5c), under the condition that all Ψ_k states below E_F are doubly occupied. La_2CuO_4 should then be a Pauli metal or a narrow-gap diamagnetic insulator if the structural distortion opens a gap at E_F. However, La_2CuO_4 is an antiferromagnetic insulator of the charge-transfer type, which implies that the b_{1g}(O−Cu)* states are singly occupied.

It is today accepted that a significant energy ($U_H \sim 5$ eV) separates the singly and doubly occupied states of Cu 3d orbitals (U_H is an on-site Hubbard Coulomb repulsion parameter, not strictly identical with the Kanamori−Brandow parameter U_{KB}, which is linked to the A, B, and C Racah parameters familiar to chemists, as U_H accounts for interatomic excitations). U_H varies with the Cu−O bond covalency and according to the nephelauxetic effect, familiar again to chemists; a decrease in the U_H value can lead to a Mott−Hubbard (insulator-to-metal) transition, familiar to physicists.

The energy difference between doubly and singly occupied 3d orbitals can be introduced in an EHTB-type approach, by adding U_H to the monoelectronic orbital energy (H_{dd}). For example, we can assume H_{dd}(doubly occupied) = −14.5 eV, corresponding to H_{dd}(singly occupied) = −18.7 eV.

Figure 7 shows the dispersion curves for $H_{dd} = -14.5$ eV, to be compared with dispersion curves in Figure 5b ($H_{dd} = -18.7$ eV).

Although O−O interactions are unchanged, significant modifications arise:

(i) Because $H_{dd}(-14.5\text{ eV}) > H_{pp}$, the classical picture for TMOs is retrieved, that is, bonding and antibonding bands are of oxygen and metal character, respectively.

(ii) With the exception of the b_{1g}(Cu−O)* band, of width (W) about 1.5 eV, the four others (around −14.5 eV) are weakly dispersed in both k and the crystal field. As previously

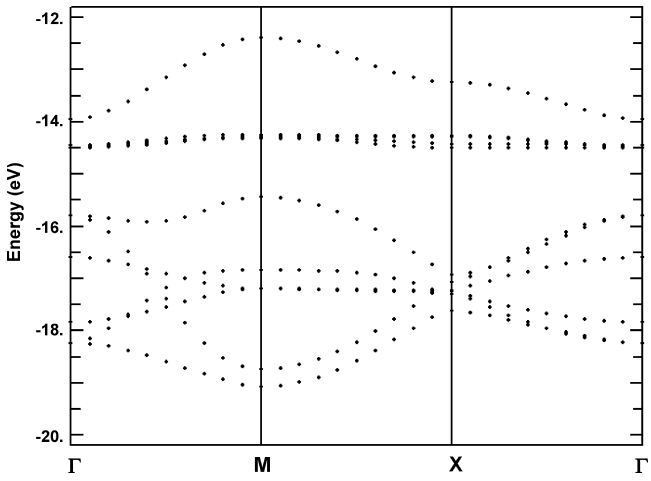

Figure 7. Same calculations as Figure 5b but using H_{dd}(Cu 3d) = −14.5 eV (i.e., $U_H \sim 4$ eV). Note that the five 3d bands lie above −14.5 eV, with b_{1g}(Cu−O)* dispersed over 1.5 eV between Γ and M.

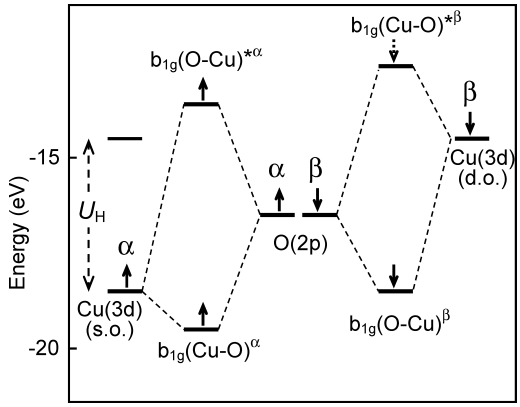

Figure 8. Molecular α and β spin orbitals for b_{1g}(Cu)−2p(O) mixing, for an energy sequence b_{1g}(singly occupied) < 2p < b_{1g}(doubly occupied), leading either to Cu or O parentage in the corresponding bonding and antibonding spin orbitals. The b_{1g}(Cu−O)* β spin orbital is occupied for Cu^+ (d^{10}).

noted, covalency largely limits the crystal-field effect. However, the half-filled character of b_{1g}(Cu−O)* still disagrees with the insulating behavior of $La_2CuO_{4.0}$.

In conclusion, Figure 7 better describes doubly occupied states, and Figure 5b better describes singly occupied states unlike most previous authors, who used $|H_{dd}| > |H_{pp}|$ only.[36] In the case of Cu^{2+}, the only singly occupied band is $b_{1g}(x^2-y^2)$. For the sake of clarity, we shall retain only singly occupied b_{1g}(Cu−O) and b_{1g}(O−Cu)* states from Figure 5b, superimposed to b_{1g}(O−Cu) and b_{1g}(Cu−O)* states from Figure 7, in a simplified "EHTB+U" scheme. This approach consists of an orbital interaction scheme, based on α and β spin orbitals, with a U_H energy difference between Cu α and β spin orbitals. O α and β spin orbitals are considered as degenerate and lie between Cu α and β spin orbitals (Figure 8), a picture related in essence to LDA+U approaches.

Figure 9a shows the main b_{1g} bands required to describe a minima the electronic structure of II+ or mixed valency (II+/III+) cuprates, in an EHTB+U approach ($U_H \sim 4$ eV).

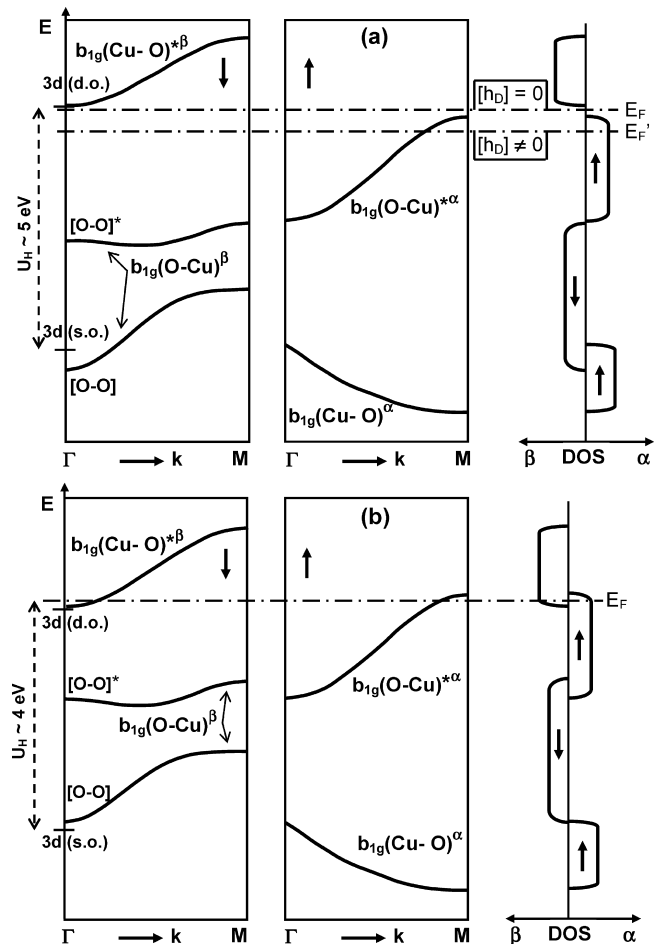

Figure 9. Selected energy bands taken from Figures 5b and 7 and corresponding to spin orbitals of Figure 8. (a) For $U_H \sim 5$ eV and undoped systems, E_F lies in a gap; E_F' corresponds to hole doping. (b) For $U_H \sim 4$ eV, b_{1g}(O−Cu)* α and b_{1g}(Cu−O)* β bands overlap at E_F.

This diagram derives from energy levels in Figures 5b, 7, and 8 and suggests the following comments:

(i) For $U_H$values larger than ∼4.5 eV, that is, the approximate width of the oxygen band, the Fermi level lies in the indirect gap between b_{1g}(O−Cu)* α_M and b_{1g}(Cu−O)* β_Γ bands. This is in agreement with the charge-transfer insulator and paramagnetic (and antiferromagnetic at low temperature) nature of $La_2CuO_{4.0}$.

(ii) Doping holes (h_D), induced by either Sr:La substitution or oxygen intercalation in the reservoir layers, arise at the top of the b_{1g}(O−Cu)* α band of oxygen character, in agreement with data from XANES experiments, as was already mentioned. The h_D hole formation is all the more stabilizing because the missing electrons are antibonding in nature (versus both Cu−O and O−O interactions).

In an ionic bonding approach, the oxidation of the $[CuO_2]^{2-}$ layer by h_D injection slightly shrinks Cu−O bonds, thus releasing the elastic strain due to the volume mismatch between the two layer types (the Goldschmidt factor comes closer to its ideal unitary value).[34]

(iii) Because of the strong oxygen character of the top of the b_{1g}(O−Cu)* α band (77% O at the M point), doping holes affect mainly oxygen, which thus adopts the oxidation number (I−) (O^- species). More precisely, the equatorial

(35) Villesuzanne, A.; Pouchard, M. C. R. *Acad. Sci. Paris Sér. IIb* **1996**, *322*, 155.
(36) Damascelli, A.; Hussain, Z.; Shen, Z. X. *Rev. Mod. Phys.* **2003**, *75*, 473.

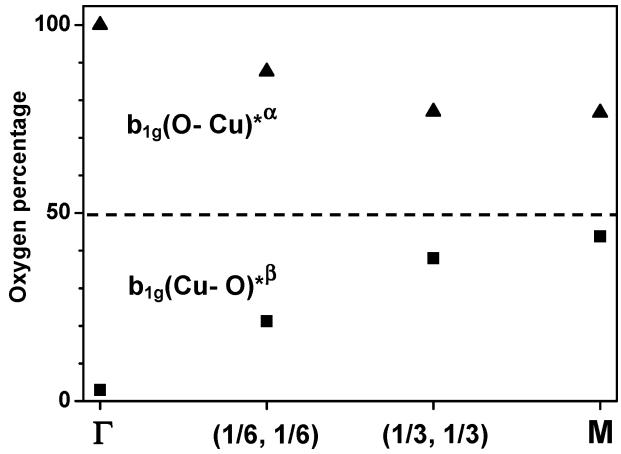

Figure 10. Oxygen percentage in the two bands b_{1g}(O−Cu)* α (HOMO) and b_{1g}(Cu−O)* β (LUMO) calculated between Γ and M. The small departure from zero for LUMO at Γ is due to the small contribution of O 2s orbitals.

oxygen oxidation number must be intermediate between I− and II−, depending on the number of O atoms sharing the doping hole.

Doping holes are of a different nature than covalency holes (h_C), induced by the oxygen contribution to the empty upper Hubbard b_{1g}(Cu−O)* β band. Zaanen, Sawatsky, and Allen (ZSA)[12] introduced covalency holes in the configuration-interaction description for Cu^{II+} in La_2CuO_4, as $a|3d^9\rangle + b|3d^{10}\underline{L}\rangle$, where $\underline{L}$ denotes a ligand hole and $a > b$.

In order to illustrate this point, Figure 10 shows the oxygen character in b_{1g}(O−Cu)* α and b_{1g}(Cu−O)* β bands as a function of the wave vector k from Γ to M in the BZ. The oxygen character is very important [up to 45% for b_{1g}(Cu−O)* β and between 77 and 100% for b_{1g}(O−Cu)* α], which justifies the ZSA description for formal Cu^{III+}, as was already mentioned in section 2.

4. From a Mixed-Valent Conductor to a Semimetal through a Mott−Hubbard-Type Transition

Hole doping (h_D) into b_{1g}(O−Cu)* α should result in a p-type metallic behavior. As in most cases of insulator-to-metal transitions, it is associated with a significant decrease of the unit cell volume ($\Delta V < 0$). It, for instance, occurs in the $LnNiO_3$ nickelate(III+) series when the lanthanide (Ln^{3+}) ionic radius, or the temperature, increases.[37,38]

(i) To this volume variation corresponds a decrease of the d_{Cu-O} and d_{O-O} interatomic distances, and therefore an increase of $|\beta_{Cu-O}|$ and $|\beta_{O-O}|$ resonance (or transfer) integrals as well as a broadening of the corresponding bandwidth ($W = 8\beta$).

(ii) To this volume variation corresponds also a decrease of the Hubbard U_H parameter because the electrons are more delocalized between Cu and O.

As a consequence, the top of the b_{1g}(O−Cu)* α band, which depends on β, goes up, whereas the bottom of the b_{1g}(Cu−O)* β band, which depends on U_H, goes down. The band gap decreases until it vanishes for a β_c critical value, and beyond this value, the Fermi level lies in the energy range where the two bands overlap: actually, the role of doping is not only to provide holes at the top of the valence band but also and mainly to favor the band overlapping.

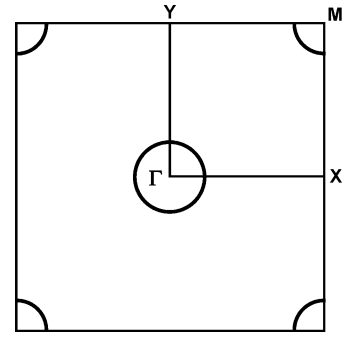

Figure 11. Fermi surface in the case of Figure 9b, with hole pockets (h_α) near M and an electron pocket (e_β) near Γ.

In the vicinity of the M point in the BZ, the occurrence of a Fermi surface [$k_F(\alpha)$] that corresponds to the empty states at the top of the b_{1g}(O−Cu)* α band is associated, beyond β_c, with a second Fermi surface [$k_F(\beta)$] around Γ that corresponds to the electrons transferred at the bottom of the b_{1g}(Cu−O)* β band. Figure 9b illustrates this situation, and Figure 11 shows the corresponding Fermi surface.

From a chemistry point of view, this electron transfer actually is of the charge-transfer type, as was previously suggested, because b_{1g}(O−Cu)* α is mainly of oxygen parentage and b_{1g}(Cu−O)* β mainly, and even purely, at Γ point, of copper parentage (cf. Figure 9b).

This transfer can be described by the "ionic" equilibrium

$$[O2]^{4-}(2p^6) + Cu^{2+}(3d^9) \leftrightarrow [O2]^{3-}(2p^{5.5}) + Cu^{+}(3d^{10})$$

shifted to the right-hand side (Δ then becomes negative).

This transfer is even more stabilizing because it transforms antibonding (unstable) electrons into almost nonbonding, more stable, electrons (close to Γ). It is expected to lead to an avalanche-type effect. Actually, in the "ionic" description of this mechanism, it can be noticed that it transforms ±2 charges into ±1 charges, which locally results in a decrease of the Madelung potentials V_M(O) and $|V_M$(Cu)|. The oxygen band is destabilized but that of copper, on the contrary, stabilized; the first one is shifted to a higher energy and the second one to a lower energy, which further accelerates the transfer process (Figure 12a).

If we consider this transfer in terms of covalency and orbital overlap through the calculated crystal orbital overlap populations (COOP), we observe that the top of the HOMO band, where the holes are created [$k_F(\alpha)$], is globally much more antibonding [in terms of both (O−Cu)* and (O−O)* interactions] than the bottom of the LUMO band [fully nonbonding at Γ and gaining progressively an antibonding (Cu−O)* character through the BZ].

However, as the transfer rate reaches a critical t_c value, this antibonding character increases rapidly (Figure 12b) and eventually limits the charge transfer.

Finally, the overlap of these two bands at the Fermi level should lead to a semimetallic situation. In the next section,

(37) Demazeau, G.; Marbeuf, A.; Pouchard, M.; Turrel, S.; Hagenmuller, P. *J. Solid State Chem.* **1971**, *3*, 582.
(38) Lacorre, P.; Torrance, J. B.; Pannetier, J.; Nazzal, A.; Wang, P. W.; Huang, T. C. *J. Solid State Chem.* **1991**, *91*, 225.

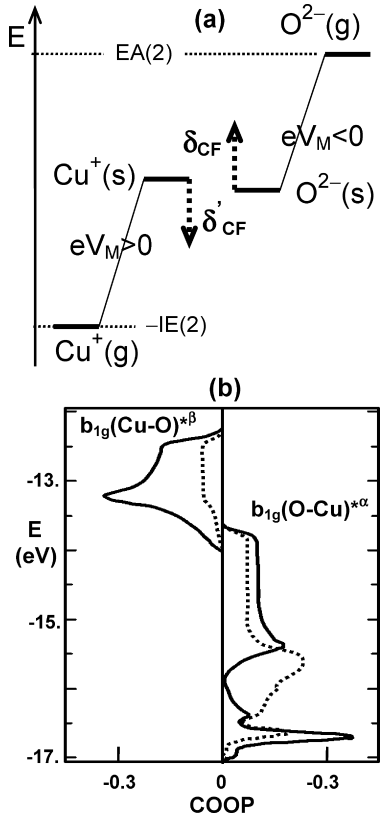

Figure 12. Avalanche-type charge transfer in terms of (a) a decrease in the crystal field, inducing a stabilization δ'_{CF} of Cu states and a destabilization δ_{CF} of O states and (b) an overlap population (COOP), calculated by the EHTB method, for Cu−O (line) and O−O (dots) interactions around E_F. The top of the b_{1g}(O−Cu)* α band has stronger antibonding character than the bottom of the b_{1g}(Cu−O)* β band.

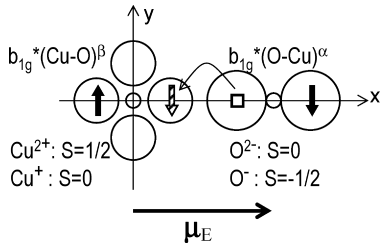

Figure 13. Schematic representation of the charge transfer from b_{1g}(O−Cu)* α to b_{1g}(Cu−O)* β states, inducing an excitonic dipole μ_E and a spin reversal. This charge transfer can also be described as a back-polarization of the Cu−O bond.

this Mott−Hubbard-type transition will be examined in a local description, based on the formation of charge-transfer excitons.

5. Excitons and Mott−Hubbard Transition

Four decades ago, Des Cloizeaux,[39] Jérome et al.,[40] and Halperin and Rice,[41] following Mott's idea[42] that, in a semimetal under certain circumstances, the electrons and holes could form bound pairs thereby leading to a nonconducting state, proposed a detailed approach of a Mott transition. They showed that when an indirect band-gap semiconductor was converted into a semimetal, or vice versa, an excitonic phase might occur at low temperature in the neighborhood of the transition (generated, for example, by pressure). Although the Hartree−Fock theory of the excitonic state is mathematically similar to the BCS theory of superconductivity, the excitonic state, which corresponds to neutral particles (an electron−hole bound as a proton and an electron in an H atom), exhibits nonsupertransport electrical properties.[41]

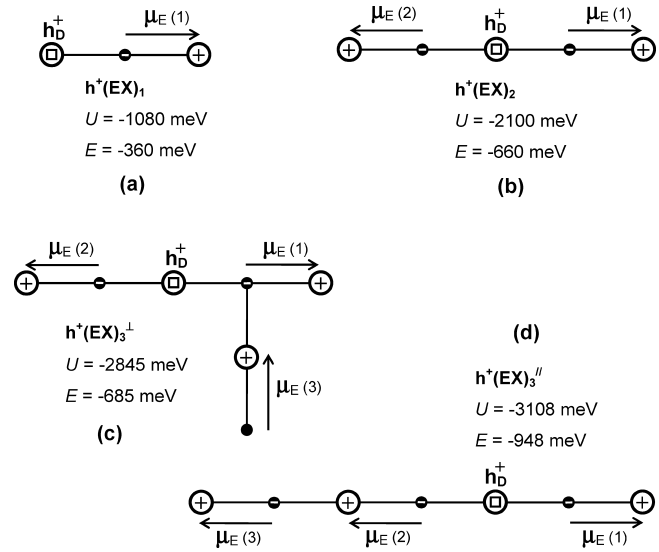

Figure 14. Coulomb attraction between the charge of a doping hole and various numbers i of surrounding excitons: (a) $i = 1$ [$h^+(EX)_1$], (b) $i = 2$ in a linear configuration [$h^+(EX)_2$], (c and d) $i = 3$ [$h^+(EX)_3$], in branched and linear configurations, respectively. The total Coulomb energy U of the dipole-doping hole system and the net interaction energy $E = U - \sum E_B$ (where E_B is the exciton binding energy) are calculated from a point-charge model (see the text).

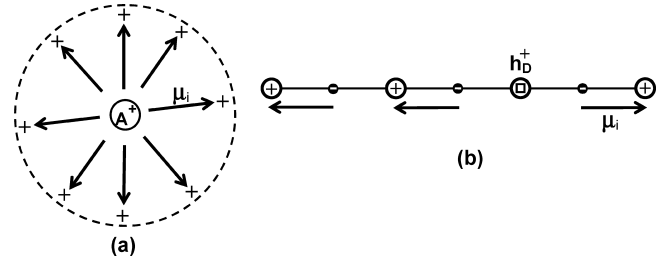

Figure 15. (a) Spherical solvation of an A^+ cation by the dipoles of polar molecules in a solvent, forming a positively charged shell. Such species can only repel each other. (b) 1D solvation of the doping hole h_D^+ by three excitons, showing the possible approach by positive (O^-) as well as negative (Cu^+) effective charges (noted by comparison to the normal charges, O^{2-} and Cu^{2+}, as in Kröger−Vink notation).

Here, we point out that our band description of hole-doped $A_2CuO_{4+\delta}$ corresponds exactly to the system studied by Halperin and Rice many years before HT_C superconductivity was discovered. The monitoring parameter in our system is the chemical pressure generated by hole doping and the negative volume variation (ΔV) due to the insulator-to-metal transition. The closure of the band gap E_G could be anticipated by an excitonic state.

The term *exciton* is used here in a broad sense. They are Frenkel-type excitons, with no large spatial extent as the

(39) Des Cloizeaux, J. *J. Phys. Chem. Solids* **1965**, *26*, 259.
(40) Jérome, D.; Rice, T. M.; Kohn, W. *Phys. Rev.* **1967**, *158*, 462.
(41) Halperin, B. I.; Rice, T. M. *Rev. Mod. Phys.* **1968**, *40*, 755.
(42) Mott, N. F. *Philos. Mag.* **1961**, *6*, 287.

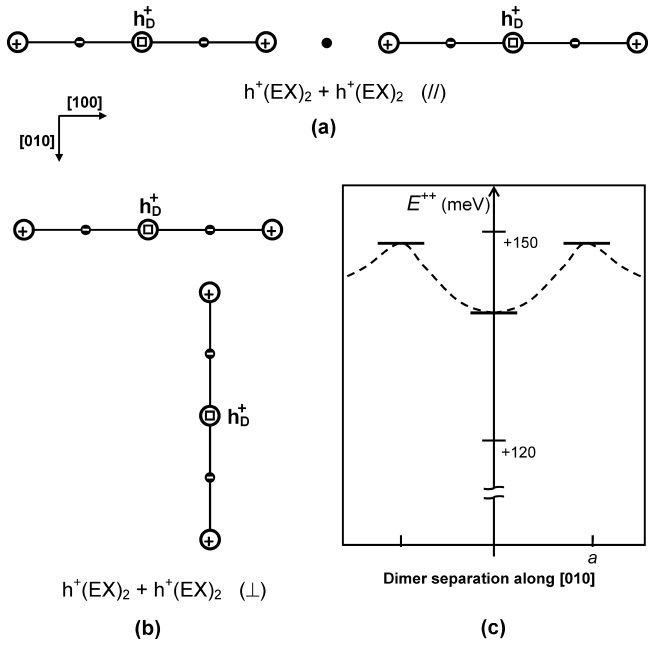

Figure 16. Various configurations of solvated $h^+(EX)_2$ entities: (a) linear configuration, involving strong repulsion ($E^{++} = 215$ meV), (b) perpendicular configuration, less repulsive ($E^{++} = 136$ meV), (c) potential well (12 meV deep) preventing the $[h^+(EX)_2]_2$ dimer separation, along the [010] direction, and inducing the "glue" between exciton-stabilized doping holes.

Mott−Wannier excitons observed in many semiconductors. They are located on two neighboring atoms (Cu and O) with a permanent electric dipole μ_E(Figure 13).

As was also mentioned by Halperin and Rice, excitons cannot form a Bose fluid but may condense into a periodic array of exciton molecules, or macromolecules, analogous to the insulating array of protons and electrons in ordinary solid hydrogen.[41]

In HT_C cuprates, the permanent dipole moment carried by the charge-transfer Frenkel exciton induces new properties because it can interact strongly with electrical charges, such as doping holes h_D^+, leading to a significant overall stabilization. From a chemical point of view, such types of interactions appear analogous to the solvation energy obtained when dissolving salt-type compounds in polar solvents. For example, sodium chloride can be dissolved in water because the hydration energy recovered by the ion−water dipole interactions can compensate for the loss of Madelung energy from the lattice destruction and so must be of the same order of magnitude. Reciprocally, the presence of doping holes h_D^+ in the cuprates is able to promote the exciton formation in neighboring sites, even before the band gap vanishes.

6. Exciton Energetics

From an ionic point of view, the charge-tranfer enthalpy ΔH can be estimated according to

$$\Delta H = -\mathrm{IE}(2) - \mathrm{EA}(2) + e\Delta V_M - e^2/d_{Cu-O}$$

where IE(2) and EA(2) are the copper second ionization energy and the oxygen second electron affinity, respectively; ΔV_M is the difference of the Madelung potential at the Cu and O sites, and the two last terms are the variation in the Madelung energy due to the electron transfer. Usually, large values of $|e|\Delta V_M$ make ΔH largely positive. Along the Mott transition, the destabilization of the top of the valence band (LHB, O^{2-} character) and the stabilization of the bottom of the conduction band (UHB, Cu^+ character) make possible the exciton formation under the condition that the doping holes bring additional negative energy ($\Delta H \leq 0$). More precisely, we can estimate the binding energy of an exciton by

$$E_B = -\frac{1}{4\pi\varepsilon_0}\frac{1}{\varepsilon_r}\frac{e^2}{d_{Cu-O}}k$$

where ε_r is the dielectric constant of the medium and $k < 1$ accounts for the partial covalent character of the Cu−O bonding. For the calculations below, we will assume $k/\varepsilon_r = 0.1$ and $d_{Cu-O} = 2$ Å to make easier comparisons between various configurations. The binding energy E_B is thus found to be −720 meV. Using a point-charge model, in which the electron is located on copper (e_{CT}^-) and the hole on oxygen (h_{CT}^+) to represent the dipole moment μ_E, it is straightforward to show that the Coulomb interaction between a doping hole h_D^+ and a simple exciton $[h^+(EX)_1]$ forming thus a tricenter species (Figure 14a) is $U[h^+(EX)_1] = -1080$ meV. This large negative value gives, for the interaction energy $E[h^+(EX)_1]$, a value of −360 meV. The same calculations taken on the $h^+(EX)_i$ species ($i = 2, 3,...$) represented on Figure 14b−d show that the [100] linear-type exciton files are the most stable, with the gain in energy per exciton decreasing only slowly down to −278 meV for $i \rightarrow \infty$. It should be mentioned that the screening of the Coulomb potential V by the conducting medium rapidly limits the spatial extent of this "spine":

$$V \propto \frac{q}{r}e^{-\lambda r}$$

where the screening length $1/\lambda$ can be estimated by the Thomas−Fermi approach. For nonlinear branched files, the total energy decreases more rapidly with the size, as mentioned in Figure 14c.

7. Exciton Topology

Many topologies of charge-exciton association can be envisaged: (i) files, linear or stairwise, with electrical dipoles aligned in the same direction ([100] or [010]), as in 1D molecular crystals, or (ii) cycle-type arrangements. These geometries prefigure the well-known charge-ordered stripes or checkerboard patches observed in cuprates and nickelates.[43,44]

We will develop these aspects in a forthcoming paper[45] dealing with linear and nonlinear topologies. Here, only $h^+(EX)_3$ and $h^+(EX)_2$ linear entities will be retained, and we will examine whether such kinds of "solvated" charges repel or attract each other.

(43) Tranquada, J. M.; Sternlieb, B. J.; Axe, J. D.; Nakamura, Y.; Uchida, S. *Nature* **1995**, *375*, 561.
(44) Hanaguri, T.; Lupieu, C.; Kohsaka, Y.; Lee, D. H.; Azuma, M.; Takano, M.; Takagi, H.; Davis, J. C. *Nature* **2004**, *430*, 1001.
(45) Pouchard, M.; Doumerc J.-P.; Villesuzanne, A. To be submitted.

For ion solvation by the polar molecules of a solvent, such an attraction between charges of the same sign is not possible: in a liquid solvent, each polar molecule is rotation- and translation-free. The charge-dipole Coulomb interactions are optimized, forming a shell of the same charge sign as that of the core ion, thus repelling each other (Figure 15a). In the cuprate crystal framework, the direction and orientation of each electrical dipole are fixed. Thus, the excitonic solvated charge $h_D^{\pm}$ should have parts of positive and negative charges, for a possible mutual attraction (Figure 15b).

We will first consider two entities $h^+(EX)_2$ getting closer to each other along the [100] direction (Figure 16a). From the calculation of the global electrostatic energy of such a dimer $[h^+(EX)_2]_2$ ($U^+ = -3985$ meV), we can evaluate the interaction energy E^{++} between the two monomers:

$$\begin{aligned} E^{++} &= U_{\text{dimer}} - 2U_{\text{monomer}} \\ &= -3985 - [-2100 \times 2] \\ &= +215 \text{ meV} \end{aligned}$$

i.e., the two entities are repelling each other.

For the same entities approaching perpendicularly along [100] and [010] as those in Figure 16b, the result ($U = -4064$ meV) gives E^{++} positive also but smaller ($E^{++} = +136$ meV). However, this configuration lies in a potential well with respect to shifting away the two entities by one cell parameter a ($U = -4052$ meV). So, the dimer cannot dissociate and remains stable, even if the ground state corresponds to both monomers in a dilute solution ($U_\infty = 2U_{\text{monomer}} = -4200$ meV; Figure 16c).

8. Conclusions

On the basis of a tight-binding+U approach for square-planar $[CuO_2]^{n-}$ 2D layers, we show that the insulator-to-metal transition, obtained by hole doping, can be of the Mott−Hubbard type, with possible closure of the band gap E_G. The occurrence of an excitonic type phase (insulating in nature) stabilizes the doping holes, in the same way as dipolar molecules in a polar solvent do, and provides the "glue" for hole pairing by means of the dipole−dipole interactions of the excitonic cloud.

Although based on the previous works by Mott, Des Cloizeaux, Jérome, Halperin, Rice, and Kohn, on the formation of excitonic phases near a Mott−Hubbard transition, and on ideas from Little, Ginzburg, Hirsch, Scalapino, or Varma, concerning virtual excitation of excitons rather than phonons, the proposed model differs from the previous works by explaining the pairing glue through exciton−exciton interactions in a nonretarded mechanism.

The bound charges can move, together with their excitonic stabilizing surroundings, because they are of electronic nature only. Such quasi-particles could be condensed in a bosonic fluid.

Such a mechanism could also apply to all of the superconducting systems presenting charge transfers, and therefore dipoles, of various types: oxygen to metal, as in cuprates and cobaltites, but also of disproportionation type, as in bismuthates, e.g., the $(Ba,K)BiO_3$ family.

Acknowledgment. This paper is dedicated to Neil Bartlett on the occasion of his 75th birthday. M.P. thanks Jacques Friedel and Philippe Nozières for fruitful discussions.

IC801031Y